BMC Cancer

RESEARCH Open Access

Identification and validation of glucose metabolism-related gene signature in endometrial cancer

Juan Jiang[1†], Nan Xia[2†], Mei Yang[3], Ping Qiu[1], Wei Zhu[1], Jing Chen[2] and Jiamei Zhu[1,3*]

Abstract

Background Metabolic syndrome associated with glucose metabolism plays a pivotal role in tumorigenesis, potentially elevating the risk of endometrial cancer (EC). This study sought to establish a glucose metabolism-related gene (GMRG) signature linked to EC.

Methods Differential analysis was conducted to identify differentially expressed genes (DEGs) between EC and normal samples from the TCGA-EC dataset. Glucose metabolism-related DEGs (GMR-DEGs) were then derived by intersecting these DEGs with GMRGs. A prognostic signature for EC was developed through the Least Absolute Shrinkage and Selection Operator (LASSO) regression and univariate Cox analysis. Additionally, immune profiling and immunotherapy responsiveness were evaluated across two distinct risk subgroups, accompanied by a single-cell analysis of prognostic genes. The expression levels of these prognostic genes were quantified at both transcriptional and translational stages using reverse transcription quantitative PCR (RT-qPCR) and immunohistochemistry (IHC) in clinical samples. Furthermore, the functional significance of key genes was explored through in vitro assays.

Results 2,912 DEGs and 202 GMR-DEGs were identified between the EC and normal groups. Subsequently, six prognostic genes were derived, including ASRGL1, SLC38A3, SLC2A1, ALDH1B1, GAD1, and GLYATL1. EC patients were classified into high and low-risk subgroups based on the six genes. Independent prognostic analysis indicated that risk score and disease stage were significant independent prognostic factors. Single-cell analysis revealed that the six prognostic genes were highly expressed in ciliated and epithelial cells. Immune cell infiltration was generally lower in the high-risk group, where tumor purity was elevated. The expression levels of SLC38A3, SLC2A1, and ASRGL1 are higher in tumor samples by RT-qPCR, with IHC confirming increased SLC38A3 expression. Finally, SLC38A3 may function as oncogenes in EC, as revealed by the results of in vitro experiments.

Conclusions In this study, we developed six novel prognostic genes in EC based on glycolysis, and corresponding prognostic models were developed. Notably, we identified SLC38A3 as the key gene, which offers valuable insights for further research into EC.

Keywords Endometrial cancer, Glucose metabolism, Prognostic signature, Risk subgroups

†Juan Jiang and Nan Xia contributed equally to this work.

*Correspondence:
Jiamei Zhu
15861039098@163.com

[1]Department of Obstetrics and Gynecology, Jingjiang People's Hospital Affiliated to Yangzhou University, Taizhou, China
[2]Department of Pathology, Jingjiang People's Hospital Affiliated to Yangzhou University, Taizhou, China
[3]Advanced Molecular Pathology, Institute of Soochow University and SANO, Suzhou, China

Introduction

Endometrial cancer (EC) represents a gynecological malignancy of growing prevalence, characterized by a consistent rise in both incidence and mortality rates [1]. Projections indicate that its incidence will escalate to 33 cases per 100,000 individuals within the next decade [2]. The growing prevalence of obesity and metabolic syndrome has contributed to an earlier onset of EC, particularly among younger individuals [3]. The International Federation of Gynecology and Obstetrics (FIGO) staging system categorizes EC into four primary stages (Stage I-IV) based on the extent of tumor growth and dissemination [4]. Early-stage EC (Stage I and II) is confined to the uterus and cervix, with no metastasis to other organs, associated with a better prognosis. Conversely, advanced-stage EC (Stage III and IV) involves metastasis to pelvic and distant organs, leading to poorer outcomes [5, 6]. Notably, 81–83% of cases are detected early [7]. The 5-year survival rate for EC is heavily dependent on the stage at diagnosis, with stage I having over a 90% survival rate, while stage IV cases see a significant drop to 14–45% [8–10]. Despite some progress in prognostic gene studies for EC, inconsistencies remain due to patient populations and sample type variations. For instance, the most hotspot POLE mutation identified in the TCGA cohort was absent in the Chinese population [11, 12]. Therefore, identifying and investigating novel molecular biomarkers is crucial to enhancing prognostic accuracy and enabling personalized therapeutic strategies.

The glucose metabolic pathway consists of three primary stages: glycolysis, oxidative phosphorylation, and the tricarboxylic acid cycle [13]. Tumor cells undergo metabolic reprogramming to increase glucose uptake and utilization, meeting the heightened energy demands for rapid proliferation [14]. Otto Warburg was the first to identify a unique metabolic profile in tumor cells, distinct from normal cells, wherein the tricarboxylic acid cycle is suppressed—now known as the Warburg Effect [15]. Under hypoxic conditions, glucose enters the cell via specific glucose transporter proteins and is predominantly converted into lactic acid [16]. Consequently, a more comprehensive understanding of glucose metabolism in the context of EC may facilitate the identification of novel therapeutic targets.

Bioinformatics has emerged as a crucial tool in enhancing diagnostic and therapeutic strategies in recent years. Prognostic prediction models, such as nomograms, facilitate the stratification of patients into distinct risk categories by incorporating clinicopathological factors alongside molecular biology data, thereby enabling tailored treatment approaches. This study identified six GMRGs through bioinformatics analysis and developed corresponding prognostic models. These prognostic genes were evaluated in clinical samples. The biological roles of key genes were further investigated through in vitro experiments. This research offers valuable insights for prognostic prediction, precise diagnosis, and potentially novel treatment strategies for patients with EC.

Materials and methods

Data source

The mRNA expression profiles and clinical data for EC were obtained from the TCGA database (https://portal.gdc.cancer.gov/). This dataset included RNA-Seq expression matrices for 554 EC samples and 35 normal samples, and corresponding clinical information for 544 EC samples. The survival data for these 544 EC samples was also downloaded as of April 27, 2023. Additionally, 202 GMRGs were curated from 18 gene sets, such as KEGG GLYCOLYSIS GLUCONEOGENESIS, WP GLYCOLYSIS, AND GLUCONEOGENESIS, as well as other gene sets of the MSigDB database. For single-cell analysis, the GSE173682 dataset, consisting of five disease subtypes of EC, was retrieved from the GEO database (https://www.ncbi.nlm.nih.gov/geo/query/acc.cgi).

Differential analysis

Using the TCGA-EC dataset and setting a threshold of adjusted p-value < 0.05 and |log2FC| > 1.5, differentially expressed genes (DEGs) between tumor and normal groups were identified via the 'DESeq2' package (version 1.36.0) [17]. Glucose metabolism-related DEGs (GMR-DEGs) were determined based on the intersection of DEGs with GMRGs.

PPI network and functional enrichment analysis

The STRING database was employed to explore the interactions among GMR-DEGs, which captures both direct physical protein interactions and indirect regulatory relationships such as co-expression and genetic interactions. These complex interactions were systematically analyzed using PPI network. Functional enrichment of Gene Ontology (GO), Kyoto Encyclopedia of Genes and Genomes (KEGG), Disease Ontology (DO), and Reactome pathways was performed using the 'clusterProfiler' package (version 4.6.0), with a significance threshold set at adjusted p-value < 0.05.

Analysis and validation of EC subgroups based on risk scores

The 544 samples from the TCGA dataset were split into training (328 cases) and testing (216 cases) cohorts in a 6:4 ratio. Univariate Cox regression and least absolute shrinkage and selection operator (LASSO) regression analyses were performed on the training cohort to identify prognostic genes based on candidate genes. To explore the precise function of prognostic genes in disease prediction, the "rms" package [18] (version 6.5-0)

was employed in the training set to develop a prognostic genes-based nomogram model for forecasting disease occurrence. This nomogram comprised of "points" and a "total score", where the former represented the scores attributed to individual prognostic genes, and the latter summed up the scores across all genes. Subsequently, we employed the "rms" package (version 6.5-0) to plot calibration curves and leveraged the pROC package [19] (version 1.18.0) to generate ROC curves, both of which were used to assess the accuracy of the model. The risk model was constructed using the following formula: $\text{risk score} = \sum_{i=1}^{n} \text{coef}(\text{gene}_i) \times \text{expr}(\text{gene}_i)$. In this formula, coef represents the risk coefficients, denotes the expression levels of each prognostic gene, i corresponds to the number of genes, and gene represents the respective prognostic gene. The survival analysis was confined to 10 years, excluding samples with survival exceeding this threshold. EC patients with available survival data were stratified into two risk subgroups, each defined by the median risk score. To assess the prognostic reliability of the model, Kaplan-Meier (K-M) survival analysis was performed at 1-, 3-, and 5-year intervals using the R package "Survival" (version 3.5-5) [20, 21]. Additionally, receiver operating characteristic (ROC) curve analysis was conducted utilizing the R package pROC (version 1.18.0) to evaluate the model's predictive capability further [22]. This identical approach was consistently applied to the training and validation sets for survival analysis and ROC assessments.

To explore the relationship between risk score and clinical variables such as age, overall survival (OS), stage, radiation therapy, pharmaceutical therapy, prior malignancy, and prior treatment, a heatmap was used to display the clinicopathological features across the two risk subgroups.

Both univariate and multivariate Cox proportional hazards regression analyses were conducted, incorporating age, OS, stage, radiation therapy, pharmaceutical therapy, prior malignancy, and prior treatment to identify independent prognostic factors. Based on these independent prognostic factors, a nomogram was constructed to predict the survival probabilities of patients with EC at 1, 3, and 5 years, with a calibration curve used to evaluate the model's predictive accuracy.

Furthermore, the correlation analysis between the prognostic genes and risk scores was conducted using the psych package (version 2.2.5) [23]. The expression levels of the prognostic genes across clinical indicators were analyzed, and the visualizations were created using ggpubr package (version 0.6.0) (https://CRAN.R-project.org/package=ggpubr).

Gene Set Enrichment Analysis (GSEA)

The 'clusterProfiler' package [24] was utilized for GSEA to explore potential pathways in different risk subgroups. The reference gene sets were GO and KEGG, with an adjusted p-value threshold of <0.05 set as the cutoff value.

Single-cell analysis

Before analyzing gene expression data from the GSE173682, single-cell transcriptomic dataset, which includes five EC groups, a comprehensive quality control (QC) procedure was performed using the Seurat R package (version 4.4.0). Filtering criteria included samples with at least 3 cells and 200 features (min. cells=3 and min. features=200). Doublets were detected using scDblFinder (version 1.16.0), and only cells with less than 10% mitochondrial content were retained. Highly variable genes were identified via the FindVariableFeatures function. Principal component analysis (PCA) was then conducted on the integrated samples using IntegrateData, and a PCA elbow plot was plotted to determine the optimal number of components capturing significant variation. Unsupervised clustering was performed using the FindNeighbors and FindClusters functions, and the clustering results were further visualized with t-Distributed Stochastic Neighbor Embedding (tSNE), offering a clearer view of cellular structure and relationships. Cell types were annotated based on known marker genes. In the GSE173682 dataset, the expression of prognostic genes was analyzed across different cell populations using ggplot2 (version 3.4.4). Cells exhibiting high expression of these prognostic genes were identified as key populations for further study.

Cellular communication and pseudo-time series analysis

A cell communication analysis was performed to quantify receptor-ligand expression and pairing between cell populations, providing insights into intercellular interactions. Using GSE173682 and annotated cell clusters, patient-specific cellular communication patterns were assessed with the CellChat package (version 1.6.1). To investigate key cell changes in cell states, a pseudo-time analysis was conducted using Monocle 2 (version 2.30.0), constructing a single-cell trajectory map that projected cells along a root-branch structure. The BEAM method in Monocle temporally ordered cells, reveals developmental trajectories and visualizes the expression patterns of prognostic genes over time.

Immune feature estimation and chemotherapy analysis

To explore the immune microenvironment in EC, the 'estimate' package was used to compute and compare Immune, Stromal, and ESTIMATE scores between the two risk subgroups. The ssGSEA algorithm was applied to

determine the relative abundance of 29 immune-related gene sets in each subgroup [25]. Expression differences in chemokines, interferons, interleukins, other cytokines, and their receptors between the two risk groups were analyzed using the 'ComplexHeatmap' package (version 2.16.0) [26]. Additionally, immune status was assessed by comparing the expression of 36 immune checkpoints and 21 HLA family genes in the two groups.

EC tissues

Between April 2023 and May 2024, 24 pairs of EC tissues and adjacent non-cancerous tissues were collected from patients undergoing surgery at the Department of Obstetrics and Gynecology of Jingjiang People's Hospital for analysis. None of the patients had received radiotherapy or chemotherapy before surgery, and informed consent was obtained from all participants. The EC tissue samples were divided into two portions: one portion was immediately frozen and stored at -80 °C for later mRNA extraction, while the other was for IHC. The study was conducted by the Declaration of Helsinki and received approval from the Ethics Committee of Jingjiang People's Hospital (Approval No. 2023-KY-019-01).

Reverse transcription quantitative PCR (RT-qPCR)

Total RNA was extracted from the tissue samples using a tissue/cell extraction kit (TIANGEN, Beijing, China). Reverse transcription was performed with the Reverse Transcription Kit (TaKaRa, Japan), and PCR amplification was conducted using the PrimeScript RT reagent Kit with gDNA Eraser (TaKaRa, Japan). Primers were synthesized by Sangon Biotech (Shanghai, China), and their sequences are provided in Supplementary Table 1. β-actin was used as the internal reference gene for calculating relative RNA expression. Each sample was tested in four identical replicate wells, and the experiments were conducted in triplicate to ensure minimal variance.

Immunohistochemistry (IHC)

For IHC, sections of EC and normal endometrial tissues were incubated overnight at 4 °C with antibodies against SLC38A3, GAD1, ALDH1B1, and GLYATL1 (1:100 dilution; Cat Nos.14315-1-AP, 10408-1-AP, 15560-1-AP, 15717-1-AP; Proteintech, China). Following primary antibody incubation, a secondary antibody was applied at a dilution of 1:200 (G1213, Servicebio, China), and visualization was achieved through DAB staining with hematoxylin used for counterstaining. The evaluation of the staining results was carried out through a double-blind assessment by two senior pathologists. A two-tier scoring system was employed:

Percentage of positive cells (per 100 cells): 0 points for no positive cells, 1 point for < 10%, 2 points for 10–50%, 3 points for 50–75%, and 4 points for > 75%.

Staining intensity: 0 points for no staining, 1 point for yellow, 2 points for brown-yellow, and 3 points for dark brown.

The final composite score was calculated by combining these two scores.

Cell lines and cell culture

The Ishikawa, AN3CA, and HEC-1 A cell lines were generously provided by the Department of Obstetrics and Gynecology at the First Affiliated Hospital of Soochow University. KLE and EEC (normal human endometrial epithelial cells) cell lines were obtained from Keycell Biotechnology Co. Ltd (Wuhan, China). For optimal cell growth and maintenance, all cell lines were cultured in a complete medium containing 10% fetal bovine serum (FBS, Gibco, USA) and 1% streptomycin-penicillin (Beyotime, Beijing, China). The Ishikawa and KLE cell lines were maintained in Dulbecco's Modified Eagle Medium (DMEM, Wuhan Pricella Biotechnology Co. Ltd), HEC-1 A was cultured in McCoy's 5 A medium (Wuhan Pricella Biotechnology Co. Ltd), and both AN3CA and EEC were cultured in Minimum Essential Medium (MEM, Wuhan Pricella Biotechnology Co. Ltd). All cell cultures were incubated at 37 °C with 5% CO_2.

Western blot analysis

Protein extraction was performed by lysing the cells on ice using RIPA lysis buffer supplemented with protease inhibitors. Protein concentrations were determined using the BCA Protein Assay Kit (Beyotime, Beijing, China). The proteins were then subjected to polyacrylamide gel electrophoresis and transferred to polyvinylidene fluoride (PVDF) membranes. Following a 2-hour blocking step at room temperature, the membranes were incubated overnight at 4 °C with an anti-SLC38A3 antibody using an anti-β-Actin antibody as the internal control. Finally, the chemiluminescent signal was amplified utilizing the ECL kit (New cell & Molecular Biotech Co., Ltd. Suzhou, China), and subsequent image analysis was conducted to quantify protein expression employing the ChemiDoc XRSVectorTM system (Bio-Rad, Hercules, CA).

Cell transfection

In the gene silencing experiments, Ishikawa cells were transfected with small interfering RNA (siRNA) targeting SLC38A3 and a negative control (NC) siRNA, utilizing the siRNA-Mate Plus transfection reagents. Vectors designed for the overexpression of SLC38A3 were constructed using the pCDNA3.1(+) plasmid and subsequently transfected into EEC cells. The empty vector, pcDNA, served as the control in this experiment. The siRNA and the SLC38A3 overexpression plasmid were obtained from Shanghai GenePharma Co., Ltd. The

target sequences for SLC38A3 siRNA are provided in Supplementary Table 2.

Cell counting Kit-8 (CCK-8) assay

Ishikawa and EEC cells harvested 24 h post-transfection were seeded into 96-well plates containing 100 µL of cell suspension (approximately 2000 cells). Each experimental group was replicated in three wells. The plates were incubated for 72 h, and at specific time points (0 h, 24 h, 48 h, and 72 h), 10 µL of CCK-8 reagent (Beyotime, Beijing, China) was added to each well. The plates were incubated for another 2 h at 37℃ before measuring at 450 nm using a microplate reader to assess cell viability.

Transwell assay

Ishikawa and EEC cells were digested 24 h after transfection, and 200 µL of an FBS-free cell suspension (3×10^5 cells) was transferred into transwell chambers with 8 µm pores (NEST, Wuxi, China). The lower chamber was filled with 600 µL of complete DMEM medium. Each experimental group was replicated in three replicate wells. After a 24-hour incubation period, migrated cells were fixed with paraformaldehyde and stained with 1% crystal violet (Beyotime, Beijing, China). The number of migrated cells was then counted under a microscope by examining at least five fields per well.

Glucose uptake, lactate production, and ATP measurement

To evaluate cellular glucose uptake, the 2-Deoxy-2-[(7-nitro-2,1,3-benzoxadiazol-4-yl) amino]-D-glucose (2-NBDG) Glucose Uptake Cell-Based Kit (Elabscience, Hubei, China) was utilized. The fluorescent marker 2-NBDG, metabolized into 2-NBDG-6-phosphate upon cellular uptake, served as a probe to measure glucose uptake. Fluorescence intensity, observed through fluorescence microscopy and flow cytometry, indicated the level of glucose uptake. Lactate concentrations in the cell homogenate supernatants were measured using the L-Lactic Acid Colorimetric Assay kit (Elabscience, Hubei, China), following the manufacturer's instructions. Additionally, ATP generation was determined by the ATP Chemiluminescence Assay Kit (Elabscience, Hubei, China).

Statistical analysis

R software (version 4.2.1) and GraphPad Prism 9 (GraphPad, Dotmatics, MA) were employed for statistical analysis. The Wilcoxon test, one-way ANOVA, or Student's t-test were used to assess the statistical significance of differences between groups. A p-value less than 0.05 was considered statistically significant.

Results

GMR-DEGs in EC

The overall study design is illustrated in Fig. 1. A sum of 2912 DEGs was identified, comprising 1641 upregulated and 1271 downregulated genes (Supplementary Fig. 1a-b). Subsequently, 39 GMR-DEGs were identified by overlapping DEGs and GRMGs (Fig. 2a), and these GMR-DEGs were visualized using volcano and heat maps (Fig. 2b-c). A PPI network of GMR-DEGs was constructed to investigate the interaction networks, which included 36 nodes and 286 edges (Fig. 2d). Functional enrichment analysis of these GMR-DEGs was then conducted. GO results revealed that the genes were primarily involved in processes such as the 'amino acid metabolic process' and 'small molecule metabolic process' (Fig. 2e). These results indicate that GMR-DEGs play essential roles in regulating metabolic pathways connected to glucose metabolism, as amino acids and small molecules often function as intermediates or regulators of glucose homeostasis. KEGG pathway analysis showed that these GMR-DEGs were mainly associated with 'Gluconeogenesis' and 'Carbon metabolism', both fundamental pathways critical for glucose production and energy balance (Fig. 2f). The enrichment of these pathways suggested that differential expression of these genes may contribute to variations in glucose metabolism-related risk scores, underlining their importance in modulating susceptibility to glucose metabolism-related risks. Additionally, Do analysis indicated an association of these genes with amino acid metabolic diseases (Fig. 2g).

Glucose metabolism-related gene signature

Univariate regression analysis of the TCGA-EC dataset identified six significant genes ($HR\neq1$ and $P<0.05$): ASRGL1, SLC38A3, SLC2A1, ALDH1B1, GAD1, and GLYATL1 (Fig. 3a). To refine the selection of prognostic genes, LASSO regression analysis was applied, resulting in the identification of the same six genes: ASRGL1, SLC38A3, SLC2A1, ALDH1B1, GAD1, and GLYATL1 (Fig. 3b-c). These genes were then used to construct a glucose metabolism-related prognostic signature for EC. Based on the median value of the risk score, EC patients with available survival data were stratified into two risk subgroups (Fig. 3d). Notably, high expression of GAD1, ASRGL1, and GLYATL1 was enriched in the low-risk EC group, while high expression of ALDH1B1, SLC38A3, and SLC2A1 was enriched in the high-risk group (Fig. 3e). Significant survival differences were observed between the two groups, with the high-risk group exhibiting poorer survival rates (Fig. 3f). To validate the model's reliability further, the AUC for predicting 1-, 3-, and 5-year survival in the training set were 0.756, 0.715, and 0.671, indicating that the model could reliably predict the survival of patients with EC (Fig. 3g).

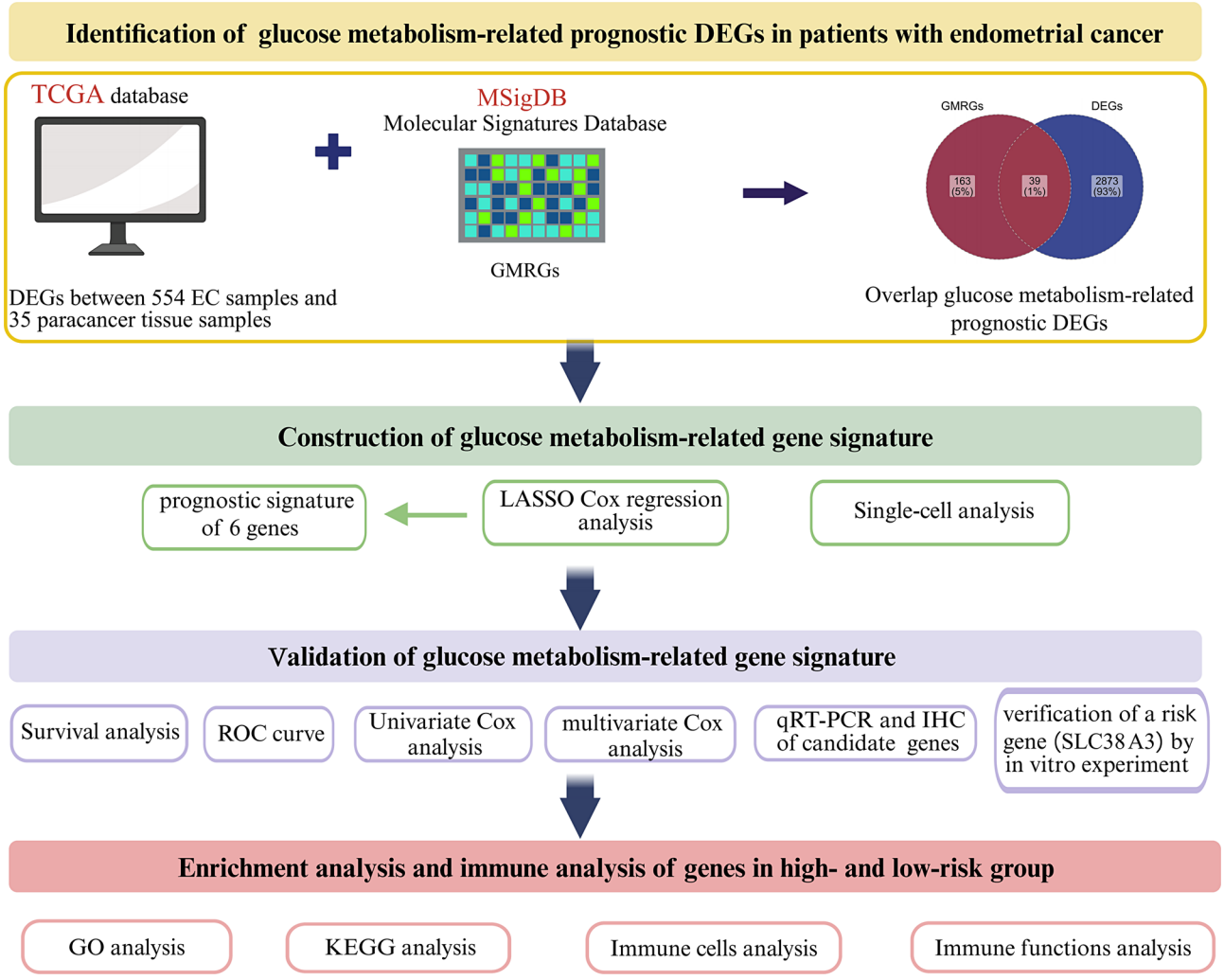

Fig. 1 The flowchart of the study

The risk model was then validated in the testing dataset. Consistent with the training set results (Fig. 4a-b), high-risk patients demonstrated a lower OS (Fig. 4c). The AUC values for the 1-, 3-, and 5-year predictions were all greater than 0.60, specifically achieving 0.716, 0.636, and 0.639 respectively (Fig. 4d). The nomogram based on 6 prognostic genes was utilized to predict the risk of developing EC in patients (Supplementary Fig. 2a). The results of the calibration curve indicated that the slope of the model curve was close to 1, and the AUC value of the ROC curve was greater than 0.9, both of which demonstrated that the constructed nomogram model had excellent predictive performance (Supplementary Fig. 2b-c).

Furthermore, ASRGL1, GAD1, and GLYATL1 demonstrated significant negative correlations with the risk score; while SLC38A3, SLC2A1, and ALDH1B1 exhibited significant positive correlations with the risk score (Supplementary Fig. 3).

Independent prognostic analysis for patients with EC

Cox regression analyses identified stage and risk score as significant independent prognostic factors ($p<0.05$) (Fig. 5a-b; Supplementary Tables 3–4). A nomogram was constructed to predict 1-, 3-, and 5-year survival rates (Fig. 5c), and its effectiveness was confirmed by the calibration curve (Fig. 5d). Additionally, risk score showed correlations with age, OS, pharmaceutical therapy, and prior malignancy (Fig. 5e; Supplementary Fig. 4). The expression analysis of the six prognostic genes in relation to clinical indicators revealed significant differences for ASRGL1 across age, OS group, Pharmaceutical Therapy group, and prior treatment group; for GAD1 across age, OS group, and Pharmaceutical Therapy group; for SLC38A3 across age, OS group, and prior malignancy group; and for SLC2A1 across OS group and Pharmaceutical Therapy group. However, none of the six genes showed significant differences between the groups in the Radiation Therapy group (Supplementary Fig. 5a-f).

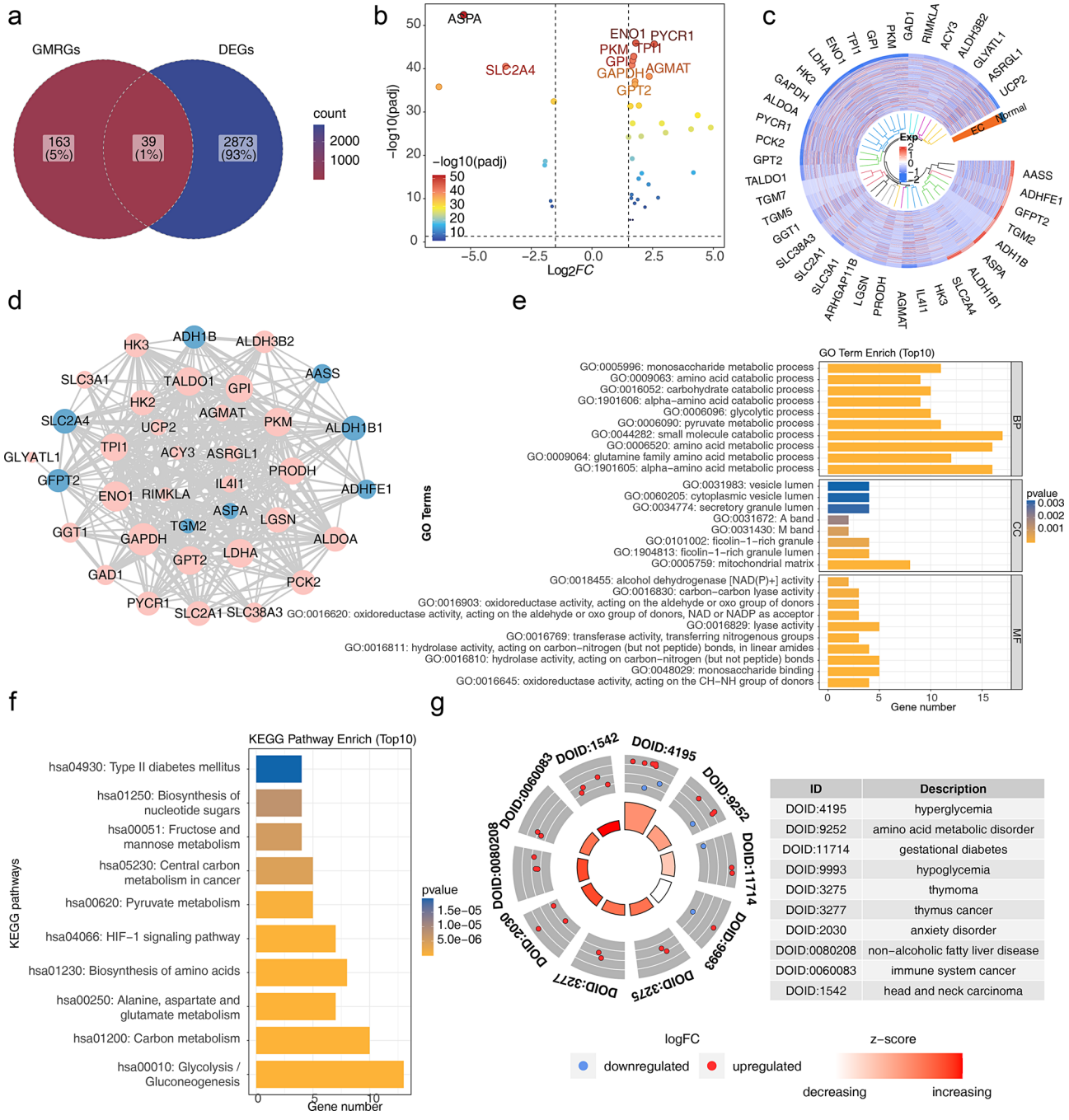

ID	Description
DOID:4195	hyperglycemia
DOID:9252	amino acid metabolic disorder
DOID:11714	gestational diabetes
DOID:9993	hypoglycemia
DOID:3275	thymoma
DOID:3277	thymus cancer
DOID:2030	anxiety disorder
DOID:0080208	non−alcoholic fatty liver disease
DOID:0060083	immune system cancer
DOID:1542	head and neck carcinoma

Fig. 2 Identification of Glucose metabolism-related DEGs in EC. (**a**) Venn diagram between DEGs and GMRGs. (**b**) The volcano plot of GMR-DEGs. The right corner indicated up-regulated genes; the left corner indicated down-regulated genes. The genes labeled in the graph are the ten most significant genes. (**c**) The heatmap of GMR-DEGs. Red indicated up-regulated genes; blue indicated down-regulated genes. (**d**) The PPI network of GMR-DEGs. Pink indicated up-regulated genes; blue indicated down-regulated genes. (**e**) GO enrichment analysis of GMR-DEGs. (**f**) KEGG and reactome enrichment analysis of GMR-DEGs. (**g**) Do enrichment analysis of GMR-DEGs

GSEA of risk subgroups

GSEA was conducted to investigate the biological pathways across various risk groups. GO analysis revealed that the low-risk group exhibited enrichment in several pathways, including 'microtubule bundle formation' and 'cilia movement' (Fig. 6a). In contrast, KEGG analysis indicated that the high-risk group was predominantly enriched in pathways related to 'Staphylococcus aureus infection' and 'neutrophil extracellular trap formation'. Conversely, the low-risk group showed significant enrichment in the 'TGF-beta signaling pathway' and 'Wnt signaling pathway' (Fig. 6b).

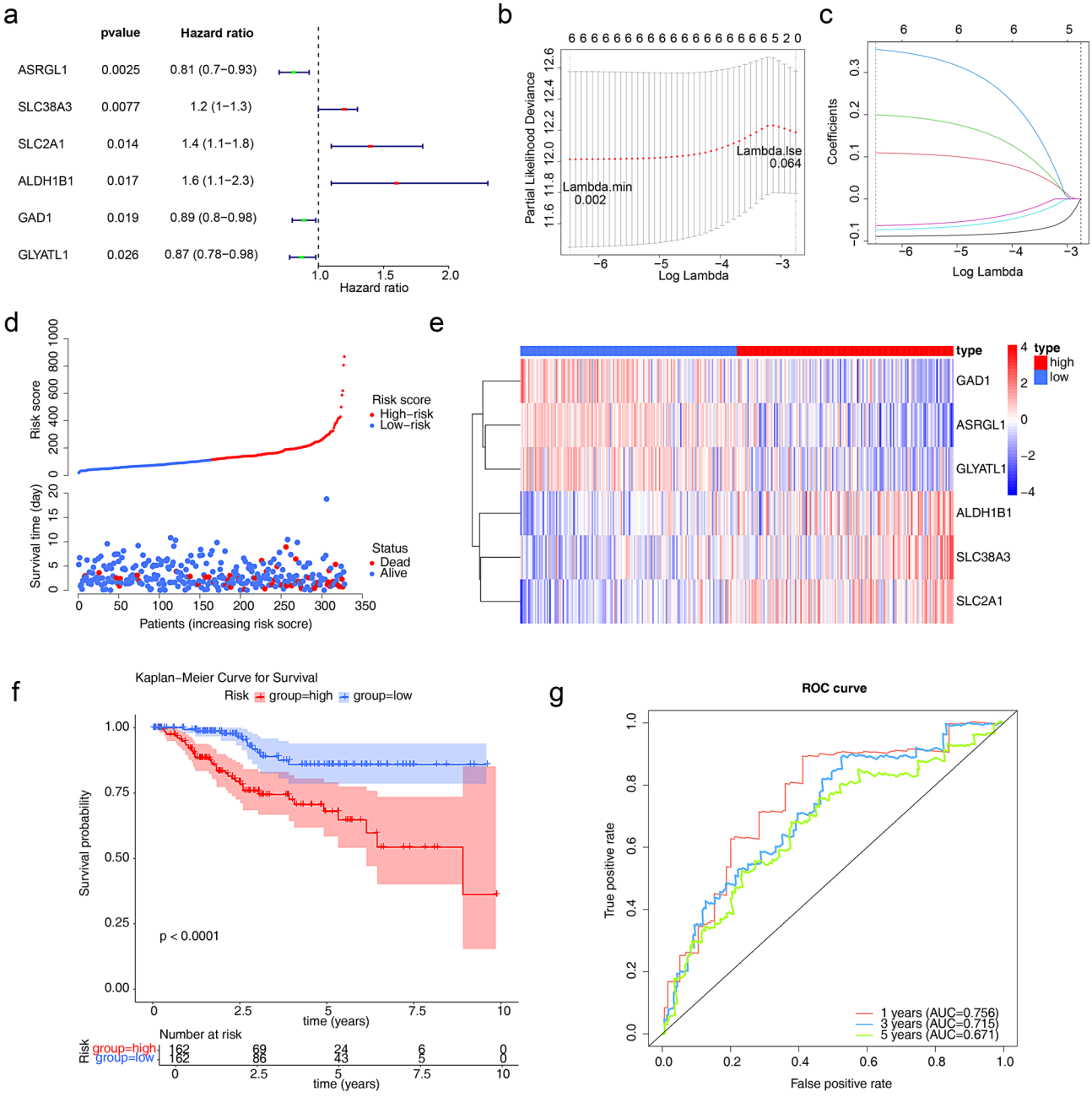

Fig. 3 Prognostic value and features of LASSO regression model in training set. (**a**) Univariate Cox regression analysis of GMR-DEGs in training set. (**b**) LASSO regression curves where each curve represented one gene. (**c**) Select the optimal parameter (lambda) in the LASSO model. (**d**) The risk score distribution of six signature genes. (**e**) The expression heatmap of six signature genes. (**f**) Kaplan Meier curves for the high-risk and low-risk groups (training set). (**g**) The survival-dependent ROC curves of the training set correspond to 1-, 3-, and 5-year

Results of single-cell and pseudotime trajectory analysis

Cell clustering and annotation analyses were performed after filtering the GSE173682 dataset (Fig. 7a). A total of 2,000 highly variable genes were identified (Fig. 7b). PCA revealed that the first 20 principal components were statistically significant. These were selected for further analyses (Fig. 7c). The cells were divided into 14 distinct clusters (Fig. 7d). The expression profiles of six prognostic genes showed elevated levels in ciliated and epithelial cells, highlighting these as key cell types (Fig. 7e-i). Cell-cell communication analysis revealed notable interactions between epithelial cells and other cell types, including macrophages, T cells, fibroblasts, endothelial cells, mast cells, B cells, and ciliated cells, with macrophages showing the strongest interaction. Ciliated cells also exhibited notable interactions with macrophages and B cells (Fig. 7j). Pseudotime trajectory analysis indicated dynamic changes in ASRGL1 and SLC2A1 expression

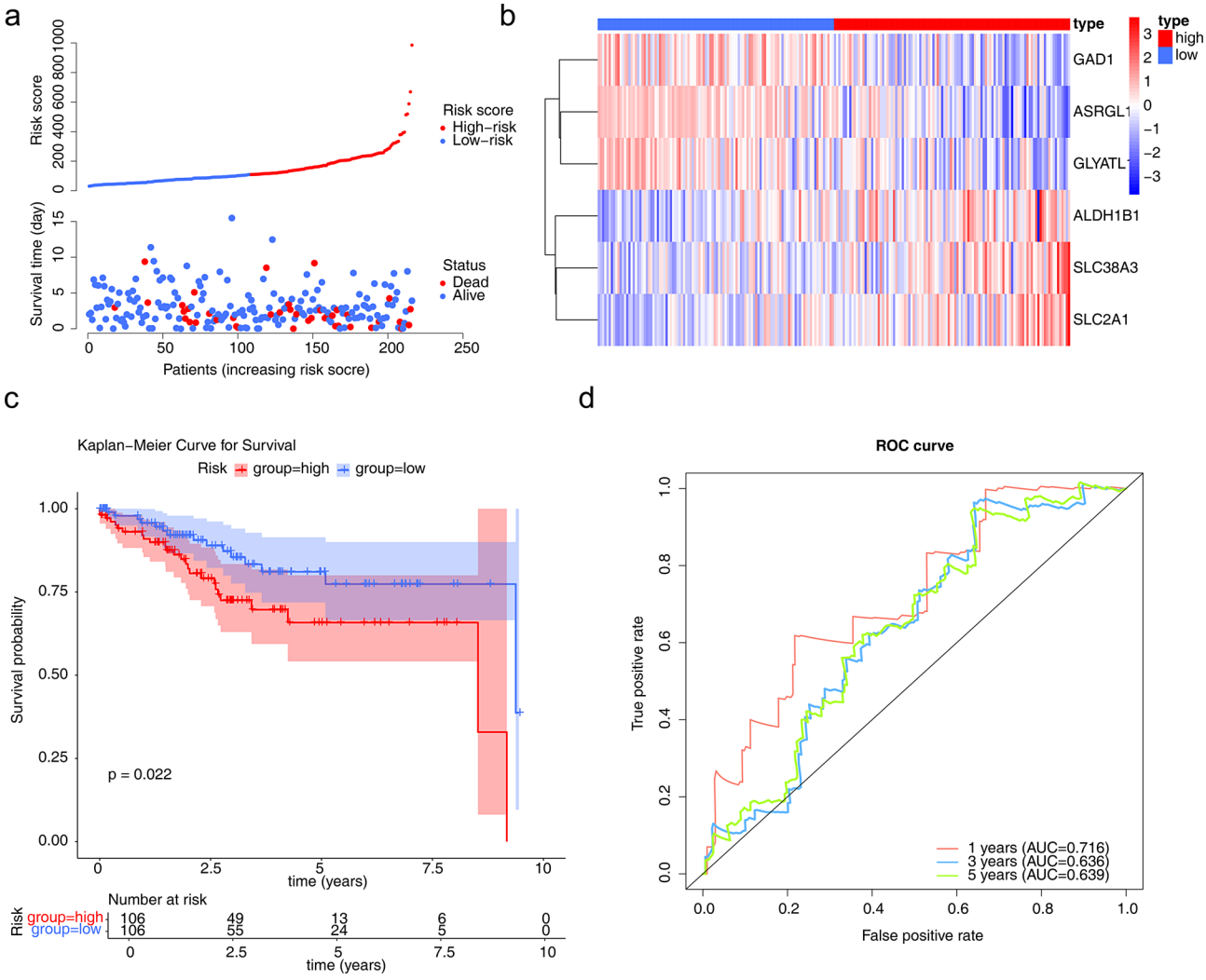

Fig. 4 Validation of the prognostic risk model in testing datasets. (**a**) The risk score distribution of six signature genes. (**b**) The expression heatmap of six signature genes. (**c**) Survival analysis of high- and low-risk groups in the testing set using Kaplan Meier curves. (**d**) The survival-dependent ROC curves of the testing set correspond to 1-, 3-, and 5-year

in both epithelial and ciliated cells. In epithelial cells, ASRGL1 expression peaked mid-phase before declining, while SLC2A1 initially increased, then decreased, and stabilized. In ciliated cells, ASRGL1 followed a similar mid-phase dip before increasing, while SLC2A1 declined early and remained stable (Fig. 7k).

Analysis of EC immune characteristics

Analysis of scores between the two risk groups revealed significantly higher ESTIMATE and immune scores in the low-risk group. At the same time, tumor purity was elevated in the high-risk group (Fig. 8a). Significant differences were observed in the abundance of eight immune cell gene sets (aDCs, B cells, $CD8^+$ T cells, iDCs, mast cells, neutrophils, T helper cells, and TIL) and nine immune function gene sets (CCR, APC co-inhibition, cytolytic activity, checkpoint, HLA, para-inflammation, T cell co-stimulation, Type I IFN response, and Type II IFN response) (Fig. 8b-c). Additionally, significant differential expression was found in 16 chemotactic factors (C3, C5AR2, CCL17, CCL19, CCL20, CCL24, CCL5, CCR5, CCR7, CXCR3, CXCR6, IL12RB1, IL16, IL18, FASLG, and GAL), three interferons (IL1R2, IL2RA, and IL2RB), and six interleukins (PLXNA4, RNASE2, SAA1, SAA2, IL2RG, and IL32) between the two risk subgroups (Fig. 8d). Moreover, 22 immune checkpoint genes and 14 HLA family genes, including CD27, CD48, and HLA-DMB, were differentially expressed (Fig. 8e-f).

Expression validation of candidate genes in clinical samples

Following bioinformatics analysis, six candidate genes were selected for RT-qPCR validation. The results showed that SLC38A3 (p=0.0191), SLC2A1 (p=0.0360),

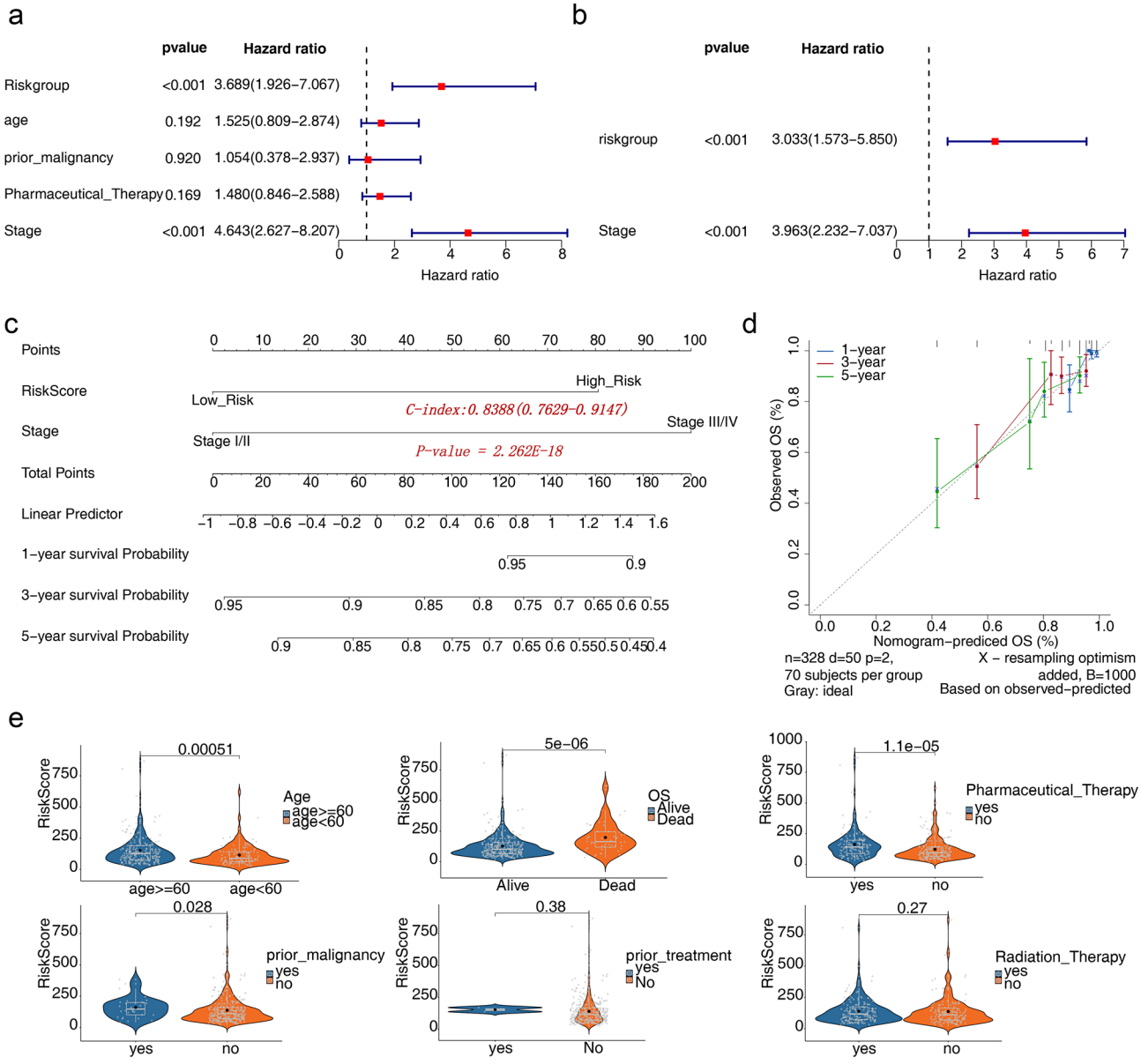

Fig. 5 Application of the signature in classifying prognosis and clinicopathological features. (**a**, **b**) Univariate (left) and multivariate (right) Cox regression analysis in the training set. (**c**) Construction of a nomogram integrated with clinicopathological characteristics. (**d**) The calibration curves based on the OS probability predicted by the nomogram. The horizontal axis represented the predicted likelihood of survival, the vertical axis represented the actual survival occurrence. (**e**) Violin plots of risk scores versus clinical characteristics

and ASRGL1 ($p=0.0287$) were significantly upregulated in EC (Fig. 9a). Although, ALDH1B1, GAD1, and GLYATL1 exhibited a trend of higher expression in EC compared to paracancerous tissues, statistical significance was not achieved. These observations align with the previous analysis of DEGs, which identified SLC38A3, SLC2A1, ASRGL1, GAD1, and GLYATL1 as upregulated in EC (Supplementary Table 5). Consequently, expanding the sample size for further validation is recommended.

Given that SLC2A1 and ASRGL1 have been previously studied in EC and their expression levels are consistent with both bioinformatics analysis and RT-qPCR results, IHC was used further to explore SLC38A3, ALDH1B1, GAD1, and GLYATL1. IHC results indicated significantly higher expression of SLC38A3 in EC tissues compared to normal tissues ($p<0.0001$) (Fig. 9b and d; Supplementary Table 6). While ALDH1B1, GAD1, and GLYATL1 also showed a trend of higher expression in EC tissues (Fig. 9b and e-g), statistical significance was not confirmed. When patients with EC were stratified by clinical stage, a recognized independent prognostic factor, expression analysis of the four candidate genes revealed that SLC38A3 was highly expressed in patients with advanced-stage EC ($p=0.0044$) (Fig. 9c), supporting the bioinformatics

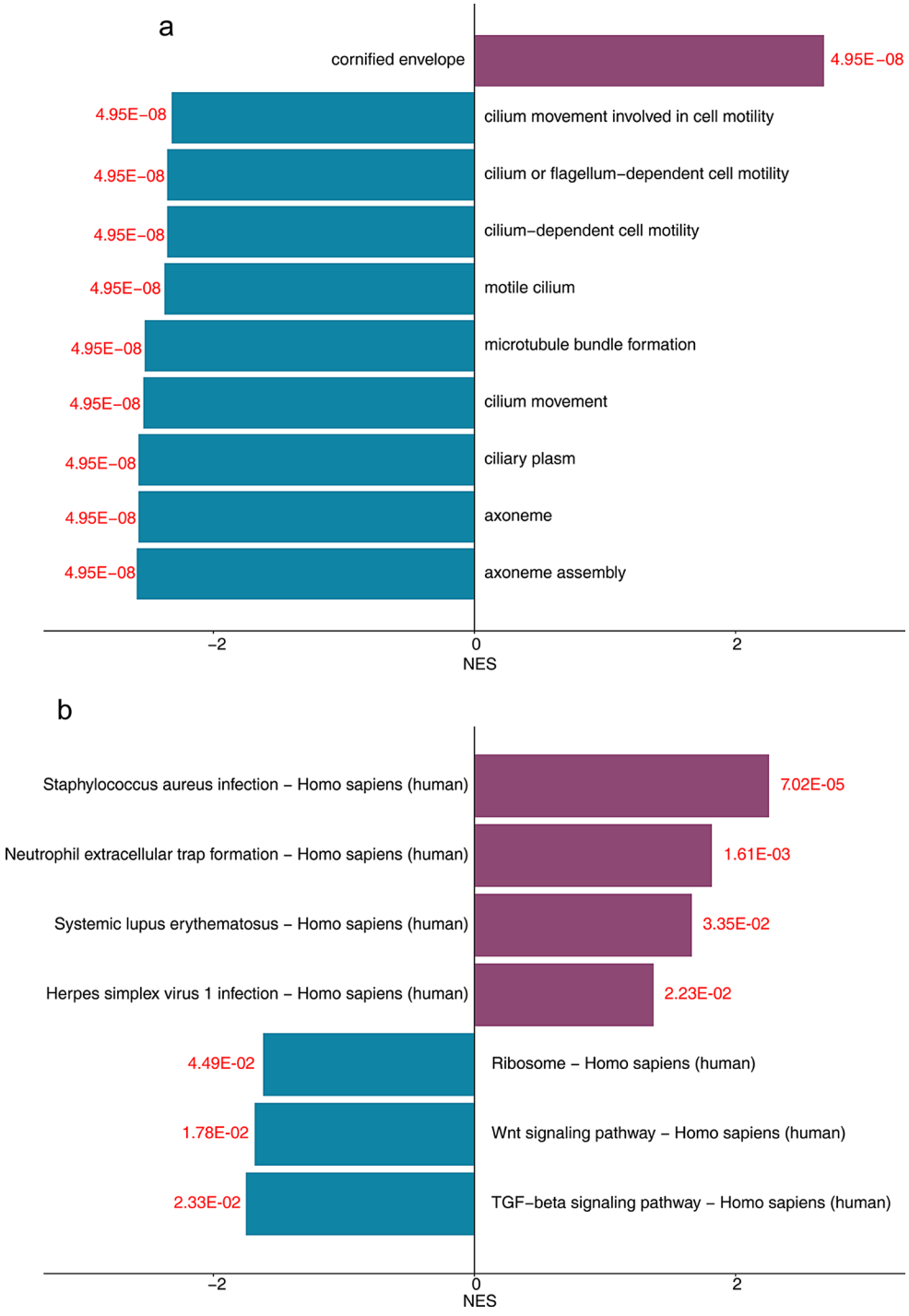

Fig. 6 GSEA analysis of risk subgroups. (**a**) GO enrichment analysis of high and low risk EC group. (**b**) KEGG enrichment analysis of high and low risk EC group

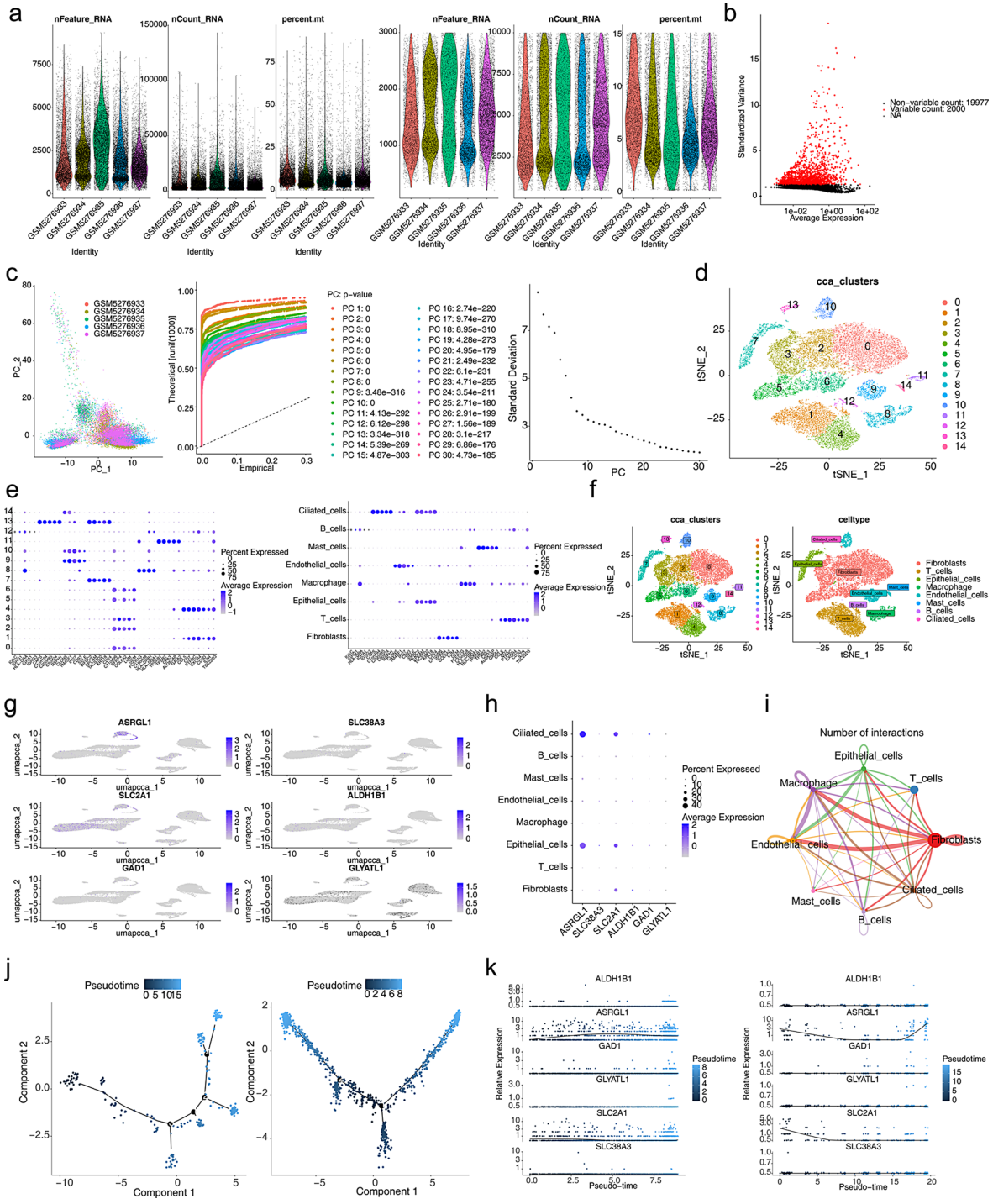

Fig. 7 Results of single-cell and pseudotime trajectory analysis. (**a-1**) Number of genes, total number of mRNA molecules, and percentage of mitochondrial genes before quality control. (**a-2**) Number of genes, total number of mRNA molecules, and percentage of mitochondrial genes after quality control. (**b**) Acquisition of highly variable genes. (**c**) Results of PCA analyses. (**d**) Results of tSNE cell clustering. (**e-1**) Plot of clustered marker gene expression points for each cell before annotation. (**e-2**) Plot of clustered marker gene expression points for each cell after annotation. (**f**) Results of tSNE cell clustering. (**g**) Clustering after cell annotation. (**h**) Expression of prognostic genes in all cells. (**i**) Expression of prognostic genes in different cells. (**j**) Intercellular communication networks in normal samples. (**k**) Results of the proposed time-series analysis of key cells

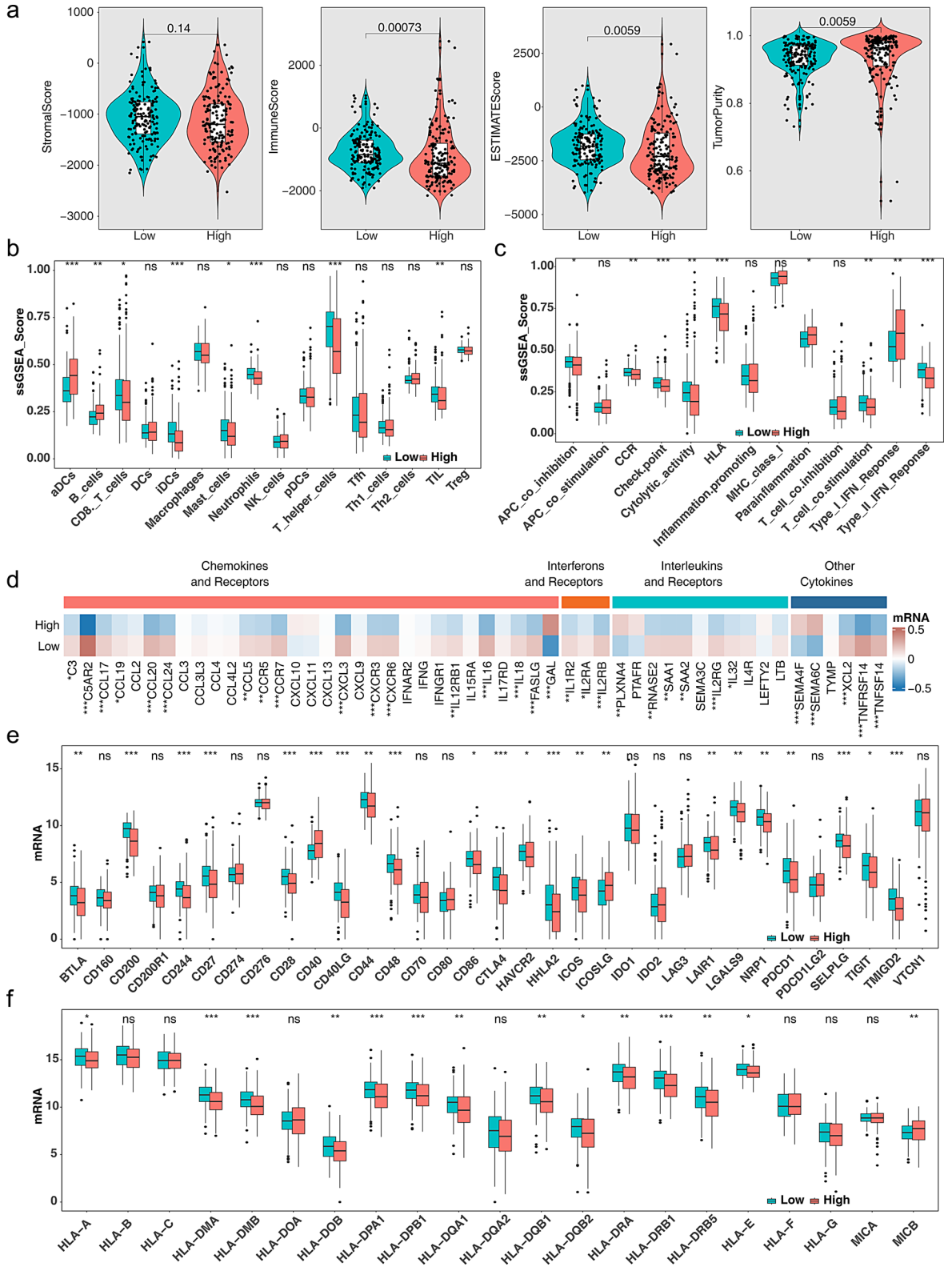

Fig. 8 Analysis of EC immune characteristics. (**a**) Violin plot of ESITMATE analysis in risk subgroups. (**b**) Boxplot of immune cell analysis in risk subgroups. (**c**) Boxplot of immune function analysis in risk subgroups. (**d**) Heatmap of the cytokines analysis in risk subgroups. (**e**) Boxplot of immune checkpoint analysis in risk subgroups. (**f**) Boxplot of HLA family genes analysis in risk subgroups

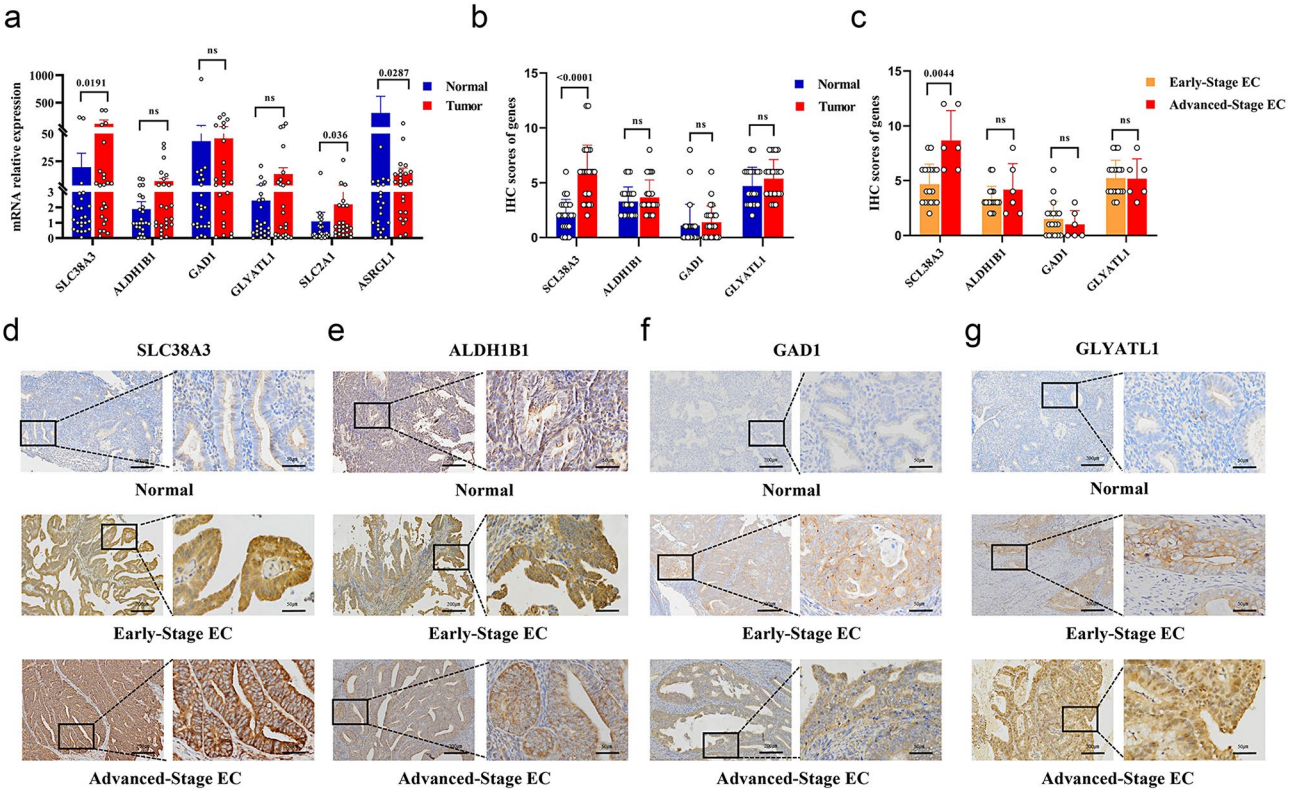

Fig. 9 Expression levels of four candidate genes. (**a**) Expression levels of six genes were analyzed using RT-qPCR. (**b**) IHC results of SLC38A3, ALDH1B1, GAD1, and GLYATL1 in tumor and normal endometrial tissue samples ($n = 24$). (**c**) IHC results of SLC38A3, ALDH1B1, GAD1, and GLYATL1 in different clinical stage EC samples. (**d**-**g**) Expression of SLC38A3, ALDH1B1, GAD1, and GLYATL1, respectively, in normal endometrial tissue samples, early-stage EC, and advanced-stage EC ($n = 24$). (100x and 400x magnification, respectively. ns, $P \geq 0.05$)

findings that SLC38A3 expression was elevated in high-risk EC group.

SLC38A3 promotes EC cells' glycolysis, proliferation, and migration

Given the strong correlation between SLC38A3 expression and prognosis, as validated by RT-qPCR and IHC, a more detailed investigation into its biological function in EC was conducted. SLC38A3 expression was analyzed in four EC cell lines (Ishikawa, HEC-1 A, KLE, AN3CA) and normal endometrial epithelial cells (EEC) using RT-qPCR and western blotting techniques. The results confirmed higher SLC38A3 expression in all EC cell lines compared to EEC, with the highest expression observed in Ishikawa cells, which were selected for subsequent analysis (Fig. 10a). To knock down SLC38A3, four siRNA sequences were designed and successfully transfected into Ishikawa cells. Both RT-qPCR and western blotting confirmed that SLC38A3-siRNA-2(si#2) and SLC38A3-siRNA-3(si#3) were most effective in reducing SLC38A3 expression (Fig. 10c). Therefore, si#2 and si#3 were selected for further experiments. Knockdown of SLC38A3 led to reduced cellular proliferation, as evidenced by the CCK8 assay (Fig. 10d), and decreased invasion capacity, as shown by the transwell invasion assay (Fig. 10e). Additionally, silencing SLC38A3 led to a decrease in glucose uptake, lactate production, and ATP generation (Fig. 10f-h). The influence of SLC38A3 on glucose metabolism and cellular growth was further substantiated through the transfection of a plasmid encoding SLC38A3 into EEC cells, thereby inducing SLC38A3 overexpression (Fig. 10b). The findings demonstrated that overexpression of SLC38A3 promoted cell proliferation, migration, and glycolytic activity, which contrasted with the effects observed following SLC38A3 knockdown (Fig. 10d-h).

Discussion

EC is a prevalent malignancy affecting the female reproductive organs, with its incidence rising rapidly, particularly in developed countries. Risk factors contributing to the development of EC include age, high BMI, metabolic syndrome, prolonged estrogen exposure, early menarche, late menopause, low parity, family history, and genetic predisposition [27]. Glycolysis represents a ubiquitous metabolic pathway within cellular processes, and conditions such as starvation and hypoxia are known to trigger metabolic reprogramming in tumor cells. This

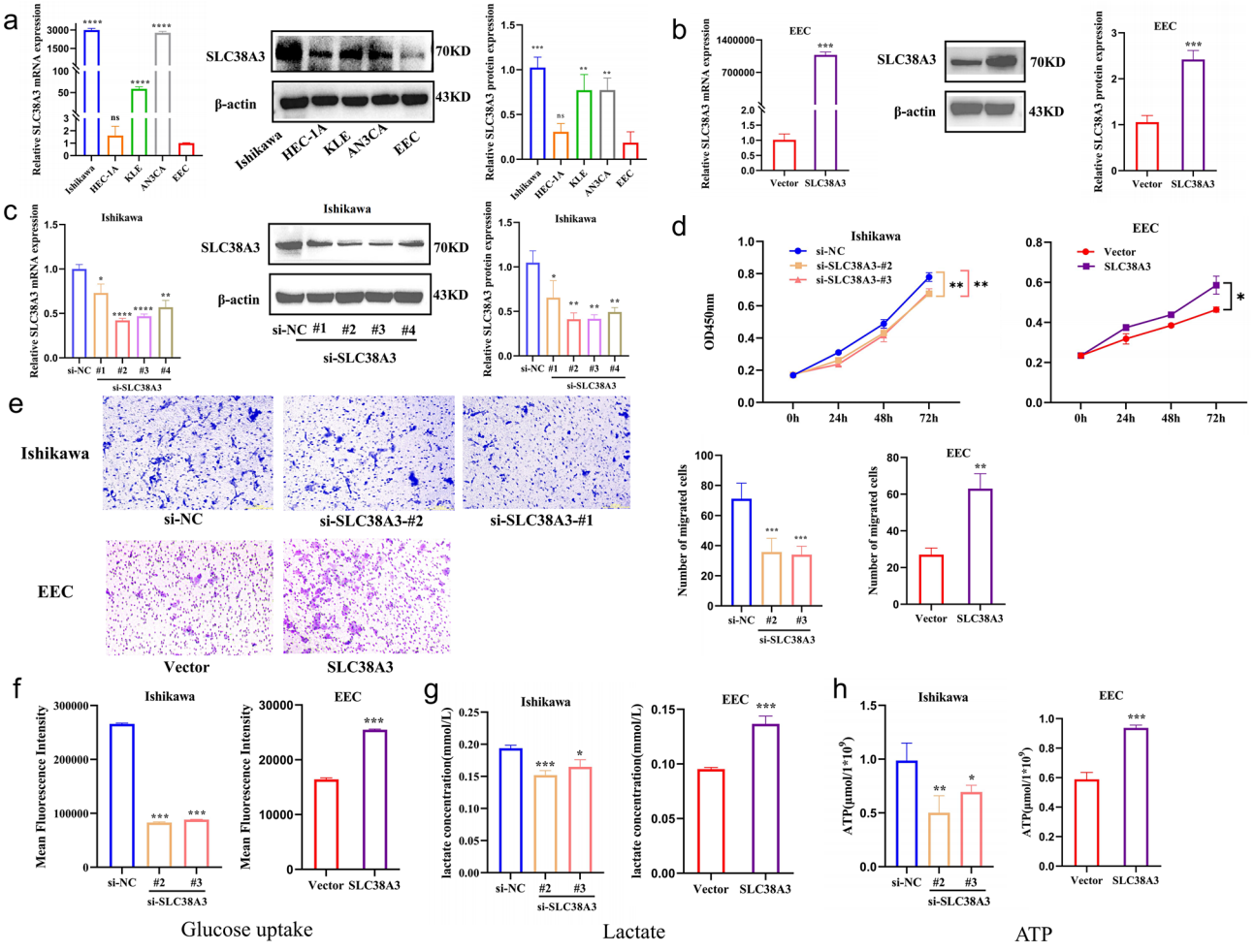

Fig. 10 Functional analysis of SLC38A3 in EC cells. (**a**) The expression of SLC38A3 in EC cells and EEC. (**b**) The overexpression efficiency of SLC38A3 in EEC cells. (**c**) The knockdown efficiency of SLC38A3 in Ishikawa cells. (**d**) The effect of SLC38A3 on the cell viability of Ishikawa and EEC cells was detected using CCK8 assays. (**e**) The effect of SLC38A3 on the migration of Ishikawa and EEC cells was detected using Transwell assays. (**f**) The effect of SLC38A3 on Ishikawa and EEC cells' glucose uptake, quantifying fluorescent intensity using the flow cytometry. (**g**) The effect of SLC38A3 on the lactate measurement of Ishikawa and EEC cells. (**h**) The effect of SLC38A3 on the ATP generation of Ishikawa and EEC cells

reprogramming is hypothesized to be linked with the pathogenesis of EC, considering the associated risk factors. In this study, we employed bioinformatics analysis to identify six GMRGs (ASRGL1, SLC38A3, SLC2A1, ALDH1B1, GAD1, and GLYATL1) that are correlated with the prognosis of EC. Utilising these genes, a prognostic model was developed, which exhibited strong predictive power, thereby underscoring its potential as an independent prognostic factor for EC patients. The stratification of patients into high- and low-risk groups based on risk factors and gene expression is of paramount importance for clinical prognosis and treatment. This approach enables physicians to personalise treatment plans, thus ensuring optimal patient care. Patients categorised as high risk may require more intensive treatment to manage disease progression, while those in the low-risk category may benefit from more conservative strategies, reducing the potential for unnecessary treatment and its associated risks.

We have identified that high expression of SLC38A3, ALDH1B1, and SLC2A1 were associated with poorer prognosis of EC. SLC38A3, a member of the SLC38 family, exhibiting a selective affinity for amino acids, particularly histidine, glutamine, aspartate, and alanine [28], contributes to metastasis in non-small cell lung cancer via activation of the PDK1/AKT signaling pathway [29]. SLC38A3 can also facilitate breast cancer progression through the GSK3β/β-catenin/epithelial-mesenchymal transition pathway [30]. Our study found that SLC38A3 mRNA and protein levels were significantly higher in EC tumor tissues, and positively correlated to the advanced stage. Functional assays demonstrated that the knockdown of SLC38A3 reduced EC cell proliferation, migration, glycolytic capacity, lactate production, and ATP generation. Conversely, the overexpression of SLC38A3

resulted in enhanced cellular proliferation and metabolic activity, highlighting its significant role in tumor progression. Although the pseudotime trajectory analysis indicates no significant changes in the expression of SLC38A3 during key cellular differentiation processes, its potential role in specific cellular states or developmental stages cannot be overlooked. Considering the experimental findings and the complexity of cellular biology, it is plausible to hypothesize that under certain pathological conditions, such as in EC, aberrant expression of SLC38A3 may drive malignant behaviors in cancer cells, potentially serving as a therapeutic target.

ALDH1B1 is highly expressed in various cancers as a mitochondrial enzyme linked to poor prognosis [31]. ALDH1B1 may also serve as a tumor stemness marker [32] and a valuable prognostic gene in cervical and colorectal cancers [33]. Our investigation aimed at quantifying the RNA expression levels of ALDH1B1 in the samples did not yield statistically significant results. We need to expand the sample size and further experimental validation of its role in EC. Numerous studies have demonstrated a strong association between SLC2A1 and tumorigenesis, indicating its role in promoting tumor cell proliferation, invasion, and migration through the facilitation of glucose metabolism [34, 35]. Furthermore, SLC2A1 expression is markedly elevated across all subtypes of endometrial cancer compared to atypical endometrial hyperplasia, which exhibits higher expression levels than normal endometrial tissue [36]. These findings align with the results of our study, suggesting that SLC2A1 may represent a viable diagnostic and therapeutic target for EC.

In addition, our bioinformatic analysis revealed a negative association between the expression of ASRGL1, GAD1, and GLYATL1 and the outcomes of EC. ASRGL1, an enzyme responsible for the hydrolysis of asparagine and glutamine into aspartate and glutamate [37], has been implicated in various cancers, including breast, prostate, and hepatocellular carcinomas [38]. Consistent with our findings, a study has identified ASRGL1 as a biomarker for lymph node metastasis in early-stage EC [39], and it has been observed that lower levels of ASRGL1 correlate with advanced EC and poorer survival rates [40, 41]. GAD1 is highly expressed in various cancers and facilitates tumor progression by modulating the tumor microenvironment [42, 43]. Our research has identified GAD1 elevated in early-stage EC relative to advanced-stage EC; however, this difference did not achieve statistical significance. Interestingly, the expression and function of GLYATL1 demonstrate variability across different cancer types. It is overexpressed in primary prostate cancer and acute myeloid leukemia, causing poor outcomes [44, 45]. Conversely, aligning with our findings, downregulation of GLYATL1 has been linked to a worse prognosis in clear cell renal cell carcinoma and hepatocellular carcinoma [46, 47]. Nonetheless, further research is required to elucidate the roles of these genes in EC comprehensively.

The survival analysis conducted in our study reveals that GAD1, ASRGL1, and GLYATL1 exhibit overexpression in the low-risk group, whereas ALDH1B1, SLC38A3, and SLC2A1 are upregulated in the high-risk group. Conversely, analysis of the TCGA dataset demonstrates that, except for ALDH1B1, nearly all these genes are expressed at higher levels in tumor tissues than in normal tissues. This observed discrepancy may be attributed to the differing methodologies employed in the two studies. This research focuses on the relationship between gene expression and patient prognosis to identify key prognostic indicators, in contrast to the TCGA, which primarily highlights the expression disparities between tumor and normal tissues. Furthermore, variations in sample characteristics, sample size, and data processing techniques may lead to statistical discrepancies, thereby complicating the interpretation of findings. Gene expression is modulated by many factors, including the tumor microenvironment, therapeutic interventions, and genetic variations, rendering it dynamic and complex. Future research should employ more advanced experimental designs and multivariable analytical approaches to enhance our understanding of these genes' roles in cancer initiation, progression, and prognosis.

Additionally, the ESTIMATE algorithm was applied to assess the potential influence of the microenvironment on different risk subgroups. The analysis revealed that the low-risk group exhibited a significantly higher immune score and was enriched in eight immune cell gene sets, suggesting that these patients may possess a more active immune microenvironment and a better response to therapy. These findings align with the prognostic model based on glucose metabolism, further supporting the link between tumor metabolism and immune function. Tumor metabolism is closely linked to the immune microenvironment, as tumor cells undergo metabolic reprogramming to produce lactate, which creates an immunosuppressive environment that promotes regulatory T cells and myeloid-derived suppressor cells while inhibiting cytotoxic T cells [48]. Glycolysis, a critical component of this metabolic reprogramming, leads to lactic acid production, which subsequently acidifies the tumor's immune microenvironment. This acidification further suppresses immune responses and facilitates tumor cell evasion from immune surveillance [49–51]. Targeting metabolic pathways could be a promising strategy to boost the effectiveness of immunotherapy. Tumor immunotherapy remains an area of intense research with considerable potential for advancement. A detailed investigation into the metabolic genes and metabolic

mechanisms involved in tumor cells could provide new insights for targeted metabolic and immune-based therapies.

Despite these insights, the study has several limitations. A primary constraint is utilizing the GSE173682 dataset, cleaning and standardizing the raw data to minimize technical variation and batch effects, and adhering to quality control standards. However, data heterogeneity remains a challenge in biological research, and future efforts will involve integrating information from additional relevant literature and databases to enhance our findings. The development and progression of EC are complex and multifactorial processes, and future studies would benefit from larger sample sizes and more refined statistical models, including multifactorial Cox regression analyses, to better capture the relationships between variables. In this study, genes were screened with a p-value threshold of <0.05, but future research could improve precision by introducing HR thresholds (>1.2 or <0.8) as an additional screening dimension. The genes GAD1, GLYATL1, and SCL38A3 exhibited statistically significant correlations, preliminarily indicating their potential involvement in disease progression regulation; however, the conclusions regarding their correlation with survival rates require further in-depth analysis. Furthermore, our investigations into SLC38A3 have been substantiated through a limited set of in vitro phenotyping experiments. A thorough comprehension of its glycolytic role and underlying mechanisms will necessitate future endeavors involving comprehensive energy metabolism evaluations, such as oxygen consumption rate and extracellular acidification rate assays, in addition to extensive in vivo studies and experimentation.

Conclusion

This study developed a risk prediction model based on six GMRGs, identified as independent prognostic factors for patients with EC, while also examining the tumor immune microenvironment. Notably, SLC38A3 was validated through RT-qPCR and IHC as highly expressed in EC samples and shown to influence EC cell growth via glycolysis. These findings lay the groundwork for future research on evaluating EC prognosis, further investigating metabolic mechanisms, and advancing immunotherapy strategies.

Abbreviations

EC	Endometrial cancer
DEGs	Differentially expressed genes
GMRGs	Glucose metabolism-related genes
GMR-DEGs	Glucose metabolism-related differentially expressed genes
LASSO	Least absolute shrinkage and selection operator
RT-qPCR	Reverse transcription quantitative PCR
BMI	Body mass index
GO	Gene Ontology
KEGG	Kyoto Encyclopedia of Genes and Genomes
DO	Disease Ontology
K-M	Kaplan-Meier
ROC	Receiver operating characteristic
OS	Overall survival
IHC	Immunohistochemistry
EMT	Epithelial-mesenchymal transition

Supplementary Information

The online version contains supplementary material available at https://doi.org/10.1186/s12885-024-13418-9.

Supplementary Material 1

Supplementary Material 2

Supplementary Material 3

Supplementary Material 4

Supplementary Material 5

Supplementary Material 6

Supplementary Material 7

Supplementary Material 8

Supplementary Material 9

Supplementary Material 10

Supplementary Material 11

Supplementary Material 12

Acknowledgements

We greatly thank the data gained from The Cancer Genome Atlas (TCGA) and Gene Expression Omnibus (GEO). Their steadfast commitment has been crucial in propelling scientific advancements. We also thank BioRender.com for their assistance with illustrations.

Author contributions

JMZ, conceived, designed, and supervised the study. JJ and NX performed data analysis and drafted the manuscript. MY helped to perform data analysis anddraft the manuscript. WZ and PQ collected the data and arranged the figures. JMZ and JC guided the experimental operation. All authors wrote and subsequently edited the original draft, which they approved as the final manuscript.

Funding

This work was supported by grants from the Scientific Research Fund Program of Jingjiang People's Hospital (JRY-KY-2023-010).

Data availability

The original contributions presented in the study are included in the article/supplementary material. Further inquiries can be directed to the corresponding author.

Declarations

Competing interests

The authors declare no competing interests.

Received: 28 July 2024 / Accepted: 31 December 2024
Published online: 07 January 2025

References

1. Siegel RL, Giaquinto AN, Jemal A. Cancer statistics, 2024. CA Cancer J Clin. 2024;74(1):12–49.
2. Xia C, Dong X, Li H, Cao M, Sun D, He S, et al. Cancer statistics in China and United States, 2022: profiles, trends, and determinants. Chin Med J (Engl). 2022;135(5):584–90.

3. Miller KD, Nogueira L, Devasia T, Mariotto AB, Yabroff KR, Jemal A, et al. Cancer treatment and survivorship statistics, 2022. CA Cancer J Clin. 2022;72(5):409–36.
4. Lu KH, Broaddus RR. Endometrial Cancer. N Engl J Med. 2020;383(21):2053–64.
5. Makker V, MacKay H, Ray-Coquard I, Levine DA, Westin SN, Aoki D, Oaknin A. Endometrial cancer. Nat Rev Dis Primers. 2021;7(1):88.
6. Homesley HD. Management of endometrial cancer. Am J Obstet Gynecol. 1996;174(2):529–34.
7. Siegel RL, Miller KD, Jemal A. Cancer statistics, 2019. CA Cancer J Clin. 2019;69(1):7–34.
8. Office for National Statistics. Cancer Survival in England. 2016.Available from: https://www.ons.gov.uk/peoplepopulationand-community/healthandsocialcare/conditionsanddiseases/bulletins/cancersurvivalinengland/adultstageatdiagnosisandchildhoodpa-tientsfollowedupto2016/previous/v1#cancer-survival-in-england-patients-diagnosed-between-2011-and-2015-and-followed-up-to-2016-national-statistics [Internet].
9. Xu Y, Burmeister C, Hanna RK, Munkarah A, Elshaikh MA. Predictors of Survival after recurrence in Women with Early-Stage Endometrial Carcinoma. Int J Gynecol Cancer. 2016;26(6):1137–42.
10. Zeng H, Chen W, Zheng R, Zhang S, Ji JS, Zou X, et al. Changing cancer survival in China during 2003-15: a pooled analysis of 17 population-based cancer registries. Lancet Glob Health. 2018;6(5):e555–67.
11. Van Gool IC, Rayner E, Osse EM, Nout RA, Creutzberg CL, Tomlinson IPM, et al. Adjuvant treatment for POLE proofreading domain-mutant cancers: sensitivity to Radiotherapy, Chemotherapy, and Nucleoside Analogues. Clin Cancer Res. 2018;24(13):3197–203.
12. Li Y, He Q, Li S, Wen X, Ye L, Wang K, Wan X. POLE mutation characteristics in a Chinese cohort with endometrial carcinoma. Onco Targets Ther. 2020;13:7305–16.
13. Jiang D, Guo J, Liu Y, Li W, Lu D. Glycolysis: an emerging regulator of osteoarthritis. Front Immunol. 2023;14:1327852.
14. Jia D, Park JH, Jung KH, Levine H, Kaipparettu BA. Elucidating the metabolic plasticity of Cancer: mitochondrial reprogramming and hybrid Metabolic States. Cells. 2018;7(3).
15. Kim JW, Dang CV. Cancer's molecular sweet tooth and the Warburg effect. Cancer Res. 2006;66(18):8927–30.
16. Xu JL, Xu Q, Wang YL, Xu D, Xu WX, Zhang HD, et al. Glucose metabolism and lncRNAs in breast cancer: Sworn friend. Cancer Med. 2023;12(4):5137–49.
17. Colaprico A, Silva TC, Olsen C, Garofano L, Cava C, Garolini D, et al. TCGAbiolinks: an R/Bioconductor package for integrative analysis of TCGA data. Nucleic Acids Res. 2016;44(8):e71.
18. Harrell FE Jr. (2023). SAHs: Regression Modeling Strategies. R package version 6.5-0. https://CRAN.R-project.org/package=SAHs
19. Robin X, Turck N, Hainard A, Tiberti N, Lisacek F, Sanchez JC, Müller M. pROC: an open-source package for R and S + to analyze and compare ROC curves. BMC Bioinformatics. 2011;12:77.
20. Therneau T. (2023). _A Package for Survival Analysis in R_. R package version 3.5-5. https://CRAN.R-project.org/package=survival
21. Terry M, Therneau, Patricia M, Grambsch. (2000). _Modeling Survival Data: Extending the Cox Model_. Springer, New York. ISBN 0-387-98784-3.
22. Robin X, Turck N, Hainard A, Tiberti N, Frédérique, Lisacek J-C, Sanchez, Müller M. (2011). pROC: an open-source package for R and S + to analyze and compare ROC curves. BMC BioinfoSAHatics, 12, p. 77.
23. Revelle. W. Psych: procedures for psychological, psychometric, and Personality Research. Northwestern University; 2024.
24. Wu T, Hu E, Xu S, Chen M, Guo P, Dai Z, et al. clusterProfiler 4.0: a universal enrichment tool for interpreting omics data. Innov (Camb). 2021;2(3):100141.
25. Charoentong P, Finotello F, Angelova M, Mayer C, Efremova M, Rieder D, et al. Pan-cancer immunogenomic analyses reveal genotype-immunophenotype relationships and predictors of response to checkpoint blockade. Cell Rep. 2017;18(1):248–62.
26. Wu Q, Tian R, Liu J, Ou C, Li Y, Fu X. Deciphering comprehensive features of tumor microenvironment controlled by chromatin regulators to predict prognosis and guide therapies in uterine corpus endometrial carcinoma. Front Immunol. 2023;14:1139126.
27. Colombo N, Creutzberg C, Amant F, Bosse T, González-Martín A, Ledermann J, et al. ESMO-ESGO-ESTRO Consensus Conference on Endometrial Cancer: diagnosis, treatment and follow-up. Ann Oncol. 2016;27(1):16–41.
28. Rubio-Aliaga I, Wagner CA. Regulation and function of the SLC38A3/SNAT3 glutamine transporter. Channels (Austin). 2016;10(6):440–52.
29. Wang Y, Fu L, Cui M, Wang Y, Xu Y, Li M, Mi J. Amino acid transporter SLC38A3 promotes metastasis of non-small cell lung cancer cells by activating PDK1. Cancer Lett. 2017;393:8–15.
30. Tan Z, Boyapati K, Tressler CM, Jenkinson NM, Glunde K. Glutamine transporter SLC38A3 promotes breast cancer metastasis via Gsk3β/β-catenin/EMT pathway. Cancer Lett. 2024;586:216653.
31. Kuang Y, Feng J, Jiang Y, Jin Q, Wang Q, Zhang C, He Y. Prognostic and immunological role of acetaldehyde dehydrogenase 1B1 in human tumors: a pan-cancer analysis. Int J Immunopathol Pharmacol. 2023;37:3946320231206966.
32. Tsochantaridis I, Roupas A, Mohlin S, Pappa A, Voulgaridou GP. The Concept of Cancer Stem cells: elaborating on ALDH1B1 as an emerging marker of Cancer Progression. Life (Basel). 2023;13(1).
33. Feng Z, Hom ME, Bearrood TE, Rosenthal ZC, Fernández D, Ondrus AE, et al. Targeting colorectal cancer with small-molecule inhibitors of ALDH1B1. Nat Chem Biol. 2022;18(10):1065–75.
34. Fu M, Liu Y, Cheng H, Xu K, Wang G. Coptis chinensis and dried ginger herb combination inhibits gastric tumor growth by interfering with glucose metabolism via LDHA and SLC2A1. J Ethnopharmacol. 2022;284:114771.
35. Freemerman AJ, Johnson AR, Sacks GN, Milner JJ, Kirk EL, Troester MA, et al. Metabolic reprogramming of macrophages: glucose transporter 1 (GLUT1)-mediated glucose metabolism drives a proinflammatory phenotype. J Biol Chem. 2014;289(11):7884–96.
36. Němejcová K, Rosmusová J, Bártů M, Důra M, Tichá I, Dundr P. Expression of Glut-1 in normal endometrium and endometrial lesions: analysis of 336 cases. Int J Surg Pathol. 2017;25(5):389–96.
37. Becker FF, Broome JD. L-asparaginase: inhibition of early mitosis in regenerating rat liver. Science. 1967;156(3782):1602–3.
38. Wang X, Wang Y, Yang L, Yuan J, Shen W, Zhang W, et al. ASRGL1 downregulation suppresses hepatocellular carcinoma tumorigenesis in a CDK1-dependent manner. Dig Liver Dis. 2023;55(7):955–66.
39. Huang CY, Liao KW, Chou CH, Shrestha S, Yang CD, Chiew MY, et al. Pilot Study to establish a Novel Five-Gene Biomarker Panel for Predicting Lymph Node Metastasis in patients with Early Stage Endometrial Cancer. Front Oncol. 2019;9:1508.
40. Edqvist PH, Huvila J, Forsström B, Talve L, Carpén O, Salvesen HB, et al. Loss of ASRGL1 expression is an independent biomarker for disease-specific survival in endometrioid endometrial carcinoma. Gynecol Oncol. 2015;137(3):529–37.
41. Fonnes T, Berg HF, Bredholt T, Edqvist PD, Sortland K, Berg A, et al. Asparaginase-like protein 1 is an independent prognostic marker in primary endometrial cancer, and is frequently lost in metastatic lesions. Gynecol Oncol. 2018;148(1):197–203.
42. Dong Y, Wang G, Nie D, Xu Y, Bai X, Lu C, et al. Tumor-derived GABA promotes lung cancer progression by influencing TAMs polarization and neovascularization. Int Immunopharmacol. 2024;126:111217.
43. Huang D, Wang Y, Thompson JW, Yin T, Alexander PB, Qin D, et al. Cancer-cell-derived GABA promotes β-catenin-mediated tumour growth and immunosuppression. Nat Cell Biol. 2022;24(2):230–41.
44. Zeng T, Huang W, Cui L, Zhu P, Lin Q, Zhang W, et al. The landscape of extrachromosomal circular DNA (eccDNA) in the normal hematopoiesis and leukemia evolution. Cell Death Discov. 2022;8(1):400.
45. Zhang Z, Chen Y, Fang L, Zhao J, Deng S. The involvement of high succinylation modification in the development of prostate cancer. Front Oncol. 2022;12:1034605.
46. Deng L, Jiang H. Decreased expression of GLYATL1 predicts poor prognosis in patients with Clear Cell Renal Cell Carcinoma. Int J Gen Med. 2023;16:3757–68.
47. Guan R, Hong W, Huang J, Peng T, Zhao Z, Lin Y, et al. The expression and prognostic value of GLYATL1 and its potential role in hepatocellular carcinoma. J Gastrointest Oncol. 2020;11(6):1305–21.
48. Chang CH, Qiu J, O'Sullivan D, Buck MD, Noguchi T, Curtis JD, et al. Metabolic competition in the Tumor Microenvironment is a driver of Cancer Progression. Cell. 2015;162(6):1229–41.
49. Cao J, Zeng F, Liao S, Cao L, Zhou Y. Effects of glycolysis on the polarization and function of tumor–associated macrophages (review). Int J Oncol. 2023;62(6).
50. Kareva I, Hahnfeldt P. The emerging hallmarks of metabolic reprogramming and immune evasion: distinct or linked? Cancer Res. 2013;73(9):2737–42.

51. Qiu X, Li Y, Zhang Z. Crosstalk between oxidative phosphorylation and immune escape in cancer: a new concept of therapeutic targets selection. Cell Oncol (Dordr). 2023;46(4):847–65.

Publisher's note